Suitability of electrochemical test methods for evaluating corrosion of the steel in alkali activated slag concretes

Qianmin Ma[a&b], Yun Bai[c], Changhui Yang[d], P. A. Muhammed Basheer[e] and Sreejith V. Nanukuttan[b*]

[a] Faculty of Civil Engineering and Mechanics, Kunming University of Science and Technology; Yunnan Provincial Key Laboratory of Civil Engineering Disaster Prevention, Jingming South Road, 650500 Kunming, China

[b] School of Natural and Built Environment, Queen's University Belfast, University Road Belfast, BT7 1NN, Northern Ireland, UK

[c] Department of Civil, Environmental & Geomatic Engineering, University College London, Gower Street, London, WC1E 6BT, UK

[d] College of Material Science and Engineering, Chongqing University, 174 Shapingba Main Street, 400044, China

[e] School of Civil Engineering, University of Leeds, England, LS2 9JT, UK

*Corresponding author's email: s.nanukuttan@qub.ac.uk

Abstract

The electrochemical tests commonly used for evaluating reinforcement corrosion in PC-based concretes may not be appropriate for testing alkali activated slag (AAS) systems due to its different pore structure and pore solution composition. In this article, corrosion behaviour of the steel bars in 12 AAS concrete mixes with different alkali concentration and modulus of sodium silicate solution was monitored by using gravimetric mass loss measurement. The

results obtained from other electrochemical tests were compared to the gravimetric mass loss to determine their suitability for assessing the corrosion of steel in AAS concretes. It was found that only 7.8-28% of the mass loss was accounted by the macrocell current for AAS concretes, indicating that this type of test underestimates the corrosion of the steel in AAS. The steel bars in the AAS concretes gave a much higher negative half-cell potential value, presumably due to the influence of sulphides. In summary, it has been established that the criteria for assessing the onset and progress of corrosion of steel in PC concretes is not suitable for the same purpose in the range of AAS concretes studied.

Key words: alkali activated slag, corrosion of steel, gravimetric mass loss, macrocell corrosion current, half-cell potential

1. Introduction

Reinforcement steel in concrete is protected from harmful substances by a passive layer of iron oxide film. Steel corrosion is known to commence when this film breaks down. The alkalinity and nature of ions in concrete pores at the steel-concrete interface have a significant influence on the stability of this passive film and therefore the initiation of corrosion (Glasser, 1991 and Broomfield, 2007). Corrosion of steel in concrete is an electrochemical process involving the formation of anodic and cathodic regions. The progress of corrosion depends on the rate of generation of electrons and ions as well as the ease of flow of these between the anode and the cathode (Broomfield, 2007). Amongst them one of the most significant factors is the ease of movement of hydroxyl ions generated at the cathodic region to the anodic region through the pore solution (Broomfield, 2007).

Alkali activated slag (AAS) is manufactured by activating ground granulated blast furnace slag (GGBS) using an alkali activator (such as sodium silicate solution) (Shi, *et al.*, 2006). Due to the nature of the raw materials, i.e., slag and alkaline activators, the pore solution chemistry and pore structure are different from that of Portland cement (PC) based concretes (Shi, *et al.*, 2006, Torres-Carrasco, *et al.*, 2015, Ma, *et al.*, 2016). Different alkali concentrations (Na_2O% of mass of slag) and modulus (Ms) of sodium silicate solution will also influence the pore solution/structure (Ma, *et al.*, 2016, Al-Otaibi, 2008, Ravikumar and Neithalath, 2013). Previously, the chloride diffusivity and bulk electrical resistivity of various AAS systems were studied and it was found that they have low diffusivity and high bulk resistivity (Ma, *et al.*, 2016, Al-Otaibi, 2008, Ravikumar and Neithalath, 2013, Tennakoon, *et al*., 2017), despite having a conductive pore solution. This would indicate a high resistance for the flow of ions from cathode to anode, so naturally a low rate of corrosion is expected. Further, the conductive pore solution and the nature of ions present in activated slag might interfere with the electrochemical test measurement.

Therefore, there is a need to assess whether there exists any variation between electrochemical measurements and actual corrosion of steel in AAS concretes and how can the criteria used for qualifying the corrosion resistance of PC concretes be used for AAS concretes. Recently, Criado and Provis (2018), Runci and Serdar (2020) and You et al. (2020) have demonstrated the corrosion behaviour of steel bars in AAS mortars under chloride environment. In the work by Criado and Provis (2018), a higher current density and a very negative corrosion potential were obtained for AAS system, while there was no visible rust on the surface of the bars embedded. Other researchers (Runci and Serdar, 2020, You. *et al*., 2020) also confirmed that AAS system showed a low chloride diffusion and a high chloride binding capacity, and then a clean surface of the bars embedded. However, a more negative corrosion potential was obtained

for such system. A systematic study was, therefore, carried out using 12 different AAS concretes when the gravimetric method of assessing the corrosion was compared with electrochemical methods, such as half-cell potential measurements and macrocell corrosion currents. The results of this study are reported in this paper and recommendations are provided for assessing the onset and rate of corrosion of steel in AAS concretes using electrochemical methods.

2. Experimental programme

As stated above, the quantification of corrosion of reinforcing steel bars in 12 AAS concrete mixes with different Na_2O% and Ms was measured by using gravimetric mass loss measurement. Corrosion current and half-cell potential of the steel bars were measured using a macrocell test set-up. The results were compared to the gravimetric mass loss to determine the suitability of these two electrochemical measurements for assessing (or quantifying) corrosion behaviour of the steel bars in the AAS concretes.

2.1 Materials

Ground Granulated Blast-furnace Slag (GGBS) provided by Civil and Marine Ltd., U. K. was used to manufacture all the AAS concretes. Class 42.5N PC conforming to British Standard EN 197-1 (2000) provided by Quinn group Ltd., U. K. was used to manufacture the PC control concrete. The chemical composition and physical properties of both the GGBS and the PC are reported in Table 1. In addition, sulphide content in the GGBS is 0.80% and chloride contents in the GGBS and the PC are 0.02% and 0.01%, respectively.

Table 1 Chemical composition and physical properties of the GGBS and the PC

	CaO	SiO_2	Al_2O_3	MgO	MnO	Fe_2O_3	K_2O	Na_2O	TiO_2	SO_3	LOI	Specific surface area (m^2/kg)	Specific gravity
GGBS	39.4	34.3	15.0	8.00	0.50	0.40	0.38	0.45	0.70	--	0.05	527	2.90
PC	61.3	23.0	6.15	1.80	--	2.95	0.68	0.22	--	2.50	1.40	286	3.16

Sodium silicate solution (or commonly known as water glass, WG) with Na_2O% of 12.45 and SiO_2% of 43.60, which is available as 'Crystal 0503' from Charles Tennant & CO (NI) Ltd., U. K. was used as the activator for GGBS. Industrial grade sodium hydroxide powder with a purity of 99% supplied by Charles Tennant & CO (NI) Ltd., U. K. was used to adjust the Ms to the required values.

A barium based retarder 'YP-1'® (Yang and Pu, 1993) was used in the AAS concretes to control their setting. The retarder was dry-blended with GGBS before mixing. The superplasticiser used in the PC concrete mix was CHEMCRETE HP3 provided by Larsen. It is a polycarboxylic polymer based superplasticiser with a water content of 40%, which was considered in proportioning the mixing water.

Crushed basalt from local sources in Northern Ireland with size fractions of 20mm and 10mm combined in a ratio of 1:1 was used as the coarse aggregate. Natural sand with fineness modulus of 2.53 was used as the fine aggregate. Water from the mains water supply was used to mix and cure the concretes (regime of curing is to be detailed in section 2.3).

2.2 Mix proportions

Twelve AAS concrete mixes with Na_2O% of 4, 6, and 8 and Ms of WG of 0.75, 1.00, 1.50 and 2.00 were investigated. The total binder content, which is the sum of GGBS and solid component in the WG, was kept constant at 400kg/m^3 for all mixes. The water-binder ratio (W/B) was constant at 0.47 for all the AAS concretes. The water content in the WG was considered in proportioning the mixing water. The retarder with dosage of 0.3% of the mass of GGBS was used to retard the setting of the AAS concretes.

For the purpose of comparison, one PC concrete mix was manufactured with the same total binder content as that of the AAS concretes. A W/B of 0.42 was determined for the PC concrete to guarantee its compliance to British Standards EN 206-1 (2000) for the exposure environments of XS3 and XD3. The use of superplasticiser at 0.4% of mass of cement allowed the PC concrete to just achieve the minimum value of conforming to class of S2 (50mm) specified in British Standard EN 206-1 (2000).

The ratio of fine aggregate to total aggregates was 36%, which was kept the same for both the PC and the AAS concretes.

2.3 Preparation of test specimens

Three 250×250×110mm blocks with a dyke on the top surface (as shown in Fig. 1) for each mix were cast for the tests to be detailed in section 2.4. For each block, four steel bars of diameter of 12mm and a length of 300mm were used to form the anode and the cathode, as shown in Fig. 1. Before embedding, the steel bars were cleaned with a wire brush and a dry cleaning cloth and then weighed. The procedure of preparation of the steel bars for macrocell corrosion test set-up is shown in Fig. 2. Approximately, 75mm of the steel bars at both ends were shielded from exposure environment (i.e., from corrosion) by applying two layers of self-amalgamating tape. Further, a rich mortar cover with a thickness of 5mm was applied over the tape. Then a layer of epoxy painting was applied onto the mortar cover. This ensured that exposure to penetrating chlorides was confined to a known area in the middle of the steel bars.

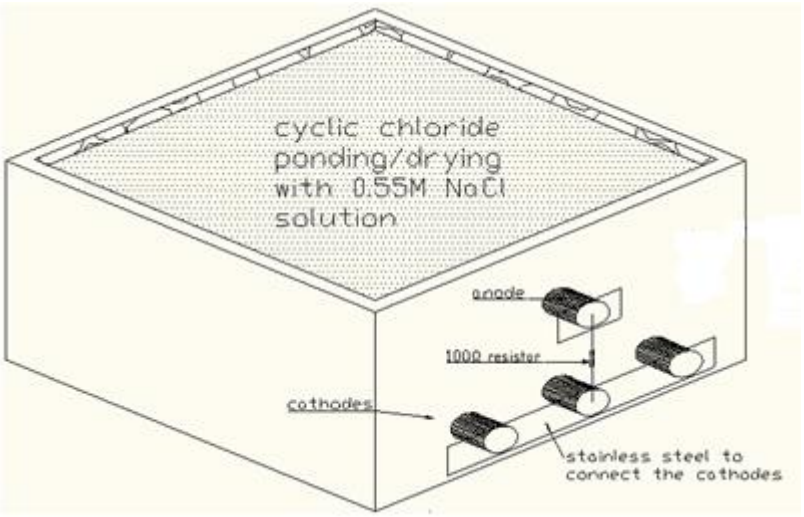

(a) Test specimen

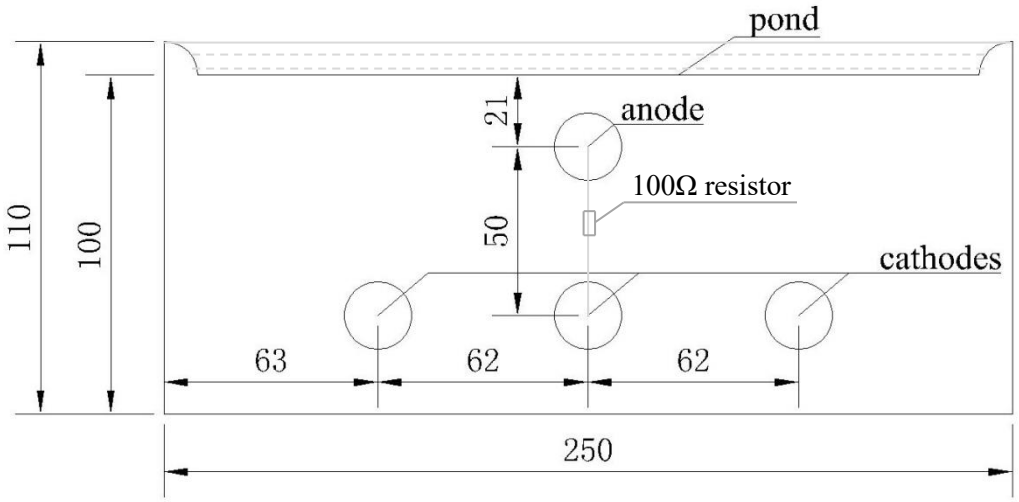

(b) Cross-section view of the concrete block in mm

Fig. 1. A sketch of the macrocell corrosion test specimen showing the location of anode, cathode and the chloride pond

(a) Steel bars

(b) Steel bars wrapped in self-amalgamating tape at both ends

(c) Casting mortar on top of self-amalgamating tape at one end

(d) Casting mortar on top of the self-amalgamating tape at the other end

(e) Steel bars with mortar end caps

(f) Epoxy painted mortar end caps

(g) Cathodic and anodic bars embedded in the mould for casting test blocks

Fig. 2. Procedure of the preparation of the steel bars before embedding in test blocks and bars in the mould for casting test blocks

The concrete blocks were cast by following the procedure given in British Standard 1881-125 (1986), in three layers with each layer receiving sufficient compaction using a table vibrator before progressing to the next layer. Further to vibration, the surface layer was finished using a metal float. The moulds were covered with thick polythene sheets to minimise evaporation of

water from the surface of concrete. Approximately 1-hour after the concrete surface hardened, the moulds were covered with layers of previously wetted hessian and polythene sheet outer layer. The samples were stored in this condition for 3 days at an average temperature of 20(±2)℃. The hessian was maintained at wet state by spraying water at every 6 hours. At the end of 3 days, the concrete specimens were demoulded, wrapped in both wet hessian and plastic bags and stored in a constant temperature room at 20(±1)℃ for 91 days. The hessian was rewetted if needed at every 2 weeks during the storage period.

In addition to the blocks for studying the corrosion, nine cubes of 100mm size were also cast for each mix by following the procedure described above.

2.4 Test procedure

2.4.1 Slump and compressive strength tests

The consistence of the concrete was measured by carrying out the slump test as per British Standard EN 12350-2 (2009). Three cubes each from the nine cubes cast for each mix were tested at the age of 3, 28 and 91 days to determine the compressive strength according to British Standard EN 12350-3 (2009).

2.4.2 Corrosion tests

One month before the test age of 91 days, the concrete blocks were moved to a constant temperature of 23±3°C and relative humidity (55±2%) chamber for conditioning the blocks for moisture for two weeks. Layers of epoxy paint were applied onto all of the surfaces of the blocks except the top surface used for ponding and the opposite bottom surface to allow the trapped air to escape. After coating the surfaces with the epoxy paint, the blocks were stored in the same conditioning room for another two weeks. Further, the anode and the cathodes was

electrically connected using a 100Ω resistor, as shown in Fig. 1. During the whole conditioning and test periods, the blocks were supported by two timber strips with a thickness of approximately 13mm so to allow air flow under the blocks. It was assumed that the test specimens did not carbonate during the period of moisture conditioning, except maybe the top 1mm, and did not interfere with the chloride transport during the ponding regime. Approximately 200ml 0.55M NaCl solution was ponded on the blocks for 1 day, which was then removed and the blocks were allowed to dry for 6 days. This cycle of ponding and drying was continued until the end of the test (~250 days). Before each ponding cycle began, half-cell potential of the anodic steel bars (at three locations from the central region of the bars) and electrical potential between the anode and the cathodes was measured by using a $Cu/CuSO_4$ half-cell apparatus and a voltmeter, respectively. Macrocell current through the circuit and further corrosion current density are calculated by using the equations below, respectively:

$$i_{mac} = \frac{1000 \cdot V}{R} \tag{1}$$

$$I_{corr} = \frac{i_{mac}}{A} \tag{2}$$

where, i_{mac} is macrocell current, μA; V is the measured electrical potential, mV; R is the electrical resistance between anodic steel and cathodic steel, 100Ω; I_{corr} is corrosion current density, $\mu A/cm^2$ and A is the surface area of the steel bars (in cm^2), which was available for exposure to chlorides and chloride induced corrosion.

The mass loss of anodic steel bar in a macrocell corrosion set-up is estimated using the following equation:

$$m = \frac{Q \cdot M}{F \cdot z} \quad (3)$$

in which,

$$Q = \int_0^t i_{mac}\, dt \quad (4)$$

where, m is mass loss of the steel, g; Q is charge passed, coulomb (notated by C); M is molar mass of steel, 56g/mol; F is Faraday's constant, 96485 coulombs/mol; z is valency of Fe, 2, i_{mac} is macrocell current, A (the μA from Eq.1 was converted A for using in Eq. 4) and t is time, s.

At the end of ponding, an area in the middle of the concrete blocks was profile ground in layers of 3mm depth to obtain concrete dust for the chloride analysis. Samples were collected up to the location of the anodic steel; that is, up to approximately 15mm from exposed surface. The total and water soluble chloride content in the dust samples was measured by using RILEM TC 178-TMC (2002a and 2002b). Further, the blocks were split opened to remove the anodic steel bars, which were then scrubbed with wire brush, wiped with a dry cloth and weighed to determine the mass loss caused by the corrosion.

2.4.3 pH measurement

After removing the anodic bars, the concrete blocks were profile ground to collect dust samples from the depths of 3mm, 6mm, 9mm, 12mm, 15mm, 20mm, 25mm, 30mm, 35mm, 40mm and 45mm. Five gram ($\pm$0.0001g) of the dust sample was then dissolved in 50 millilitre of deionised water in a glass beaker by stirring the content of 3 minutes. The pH of this suspension was measured using a pH meter, which is reported as apparent pH. The apparent pH was plotted against the depth to obtain the pH profile at the end of the cyclic ponding test.

3. Results and discussion

3.1 Slump and compressive strength

The slump and compressive strength of all the 13 mixes were reported in our previous paper (Ma, *et al*., 2016) which are reported here in Table 2. As stated earlier, a retarder of 0.3% by mass of slag was used for the AAS mixes whilst superplasticiser of 0.5% by mass of cement was used for PC mix. The water-binder ratio of the AAS concretes was 0.47 whereas it was 0.42 for the PC concrete.

As reported in the previous paper (Ma, *et al*., 2016), all the mixes satisfied the minimum slump of 50mm for their use in marine environments (British Standard 8500-1, 2006). However, it was found that the addition of the retarder and the use of slightly higher water-binder ratio in the AAS concretes had a slightly detrimental effect on the compressive strength, particularly at the age of 3d. The mixes were expected to meet the requirement for XS3 and XD3 exposure environments specified in British Standard EN 206-1 (2000) as the PC reference concrete was designed to satisfy this requirement. The compressive strength at the age of 28 days suggests that not all the AAS concretes achieved the required strength of 58MPa for the two exposure classes. However, most of the AAS concretes met the strength requirement of 50MPa for the exposure classes XS1, XD1 and XD2. At the time of carrying out this research, a suitable admixture that could be used to control the workability of the AAS concretes was not available, but it is expected that with the availability of new admixtures specifically for use with AAS and geopolymer systems from different manufacturers, the above limitation could be addressed.

Table 2 Slump and compressive strength (±standard deviation) of the concrete mixes

Mix ID (Na_2O%-Ms)	**Slump (mm)**	**Compressive strength (MPa)**		
		3 day	**28 day**	**91 day**
4%-0.75	55	22.3±0.1	44.7±0.2	46.4±1.0
4%-1.00	55	21.8±0.1	46.7±1.0	55.6±0.6
4%-1.50	55	1.7±0.0	49.5±0.2	52.6±2.3
4%-2.00	55	1.4±0.0	33.3±0.4	44.1±0.1
6%-0.75	65	31.7±0.7	47.3±0.0	51.8±2.4
6%-1.00	65	37.3±0.2	53.6±0.0	59.1±0.8
6%-1.50	65	20.3±0.7	60.8±0.1	67.4±2.6
6%-2.00	75	8.0±0.0	59.6±0.2	68.7±2.1
8%-0.75	70	32.3±0.0	51.9±0.1	56.2±0.2
8%-1.00	105	32.7±2.4	53.6±0.1	67.1±0.6
8%-1.50	145	34.1±0.7	59.3±3.2	70.5±2.5
8%-2.00	180	11.7±0.2	55.4±0.2	65.0±0.8
PC	50	35.4±1.2	58.9±1.8	66.3±2.3

3.2 Apparent pH

Fig. 3 shows the apparent pH profiles of concretes after the cyclic ponding test. It can be seen that the alkalinity of the AAS concretes was considerably lower in the surface zone (15mm) compared to the PC concrete. This reduction is considered to have been caused by the outward diffusion of alkaline materials from the AAS concretes and the partial carbonation of the near surface of concrete during the conditioning stage before exposing to chlorides. As the

concentration of sodium ions in the exposure solution was high, the outward diffusion of sodium ions from AAS concretes could not have happened. Therefore, the outward diffusion of potassium, calcium and hydroxyl ions is mainly responsible for the reduction in alkalinity. However, $Ca(OH)_2$ is not one of the hydration products of the AAS concretes. Therefore, the continuous outward diffusion of the alkaline materials in AAS concretes could also result in the dissolution of the hydration products of the AAS concretes, such as C-S-H gels (Johannesson, *et al*., 2007), which was confirmed in this study with the presence of exposed aggregates at the end of the ponding test. In the PC concrete, $Ca(OH)_2$ would dissolve in the pore solution to buffer the alkalinity when the outward diffusion of alkaline materials occurs, resulting in the trend seen in Fig. 3.

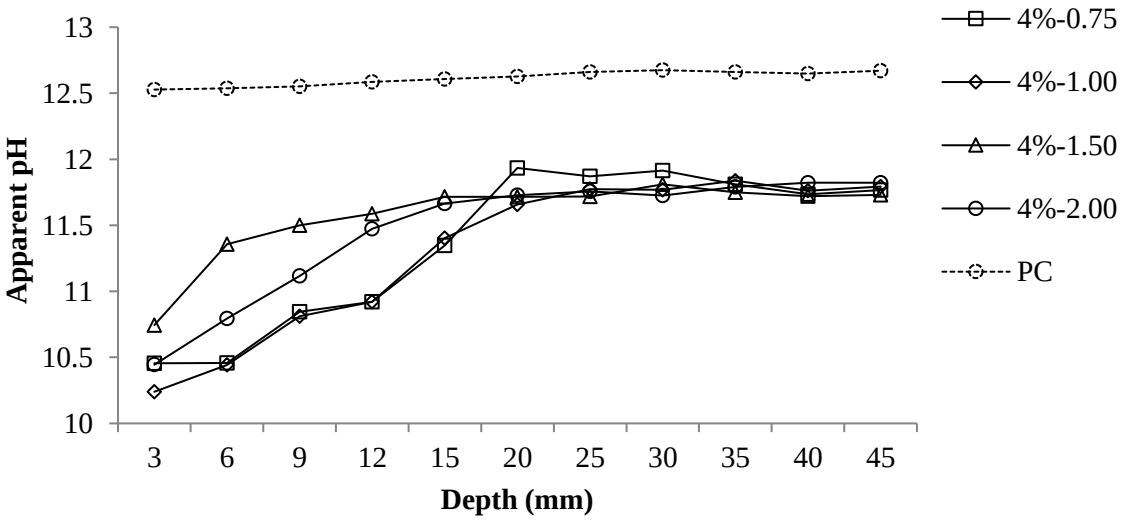

(a)

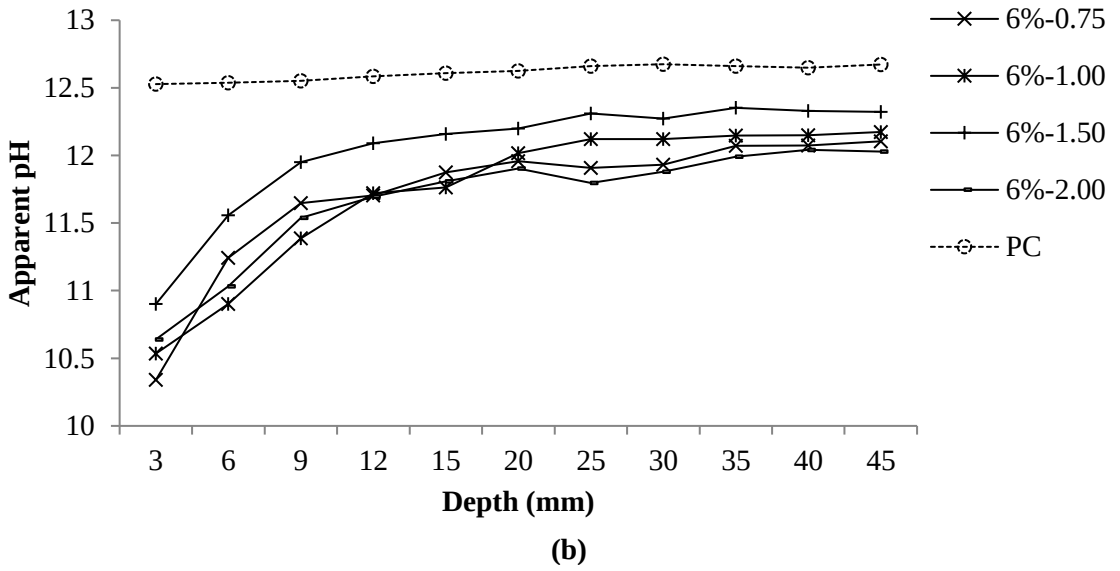

(b)

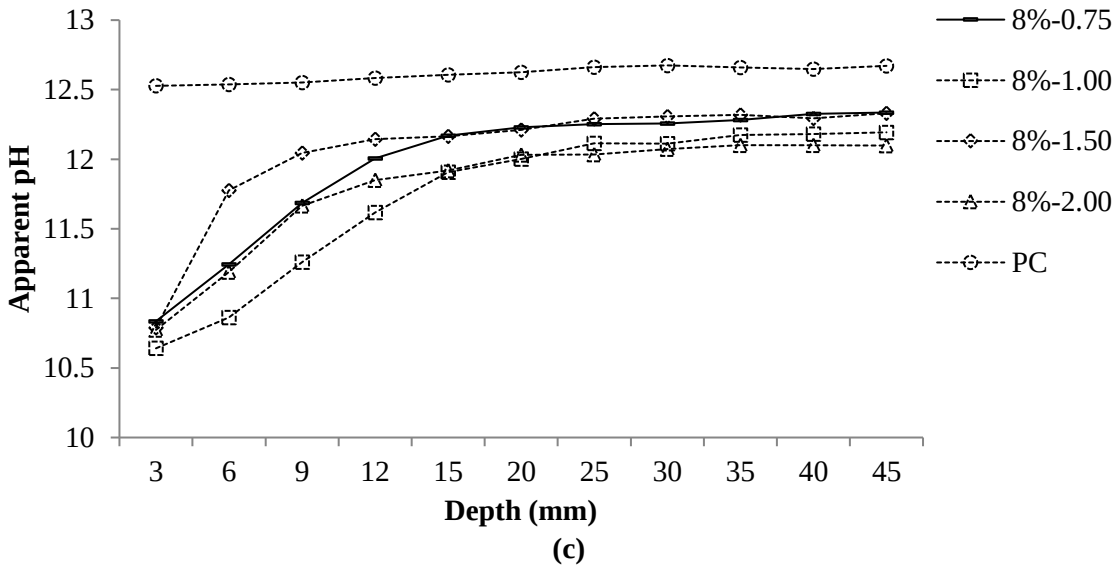

(c)

Fig. 3 Apparent pH profiles of the concretes after the cyclic ponding test (the anodic steel bar was at 15mm depth in all cases)

3.3 Macrocell current

Fig. 4 presents the evolution of corrosion current density ($\mu A/cm^2$) and the charge passed (Coulomb - C) for the 12 AAS concretes and the PC reference concrete.

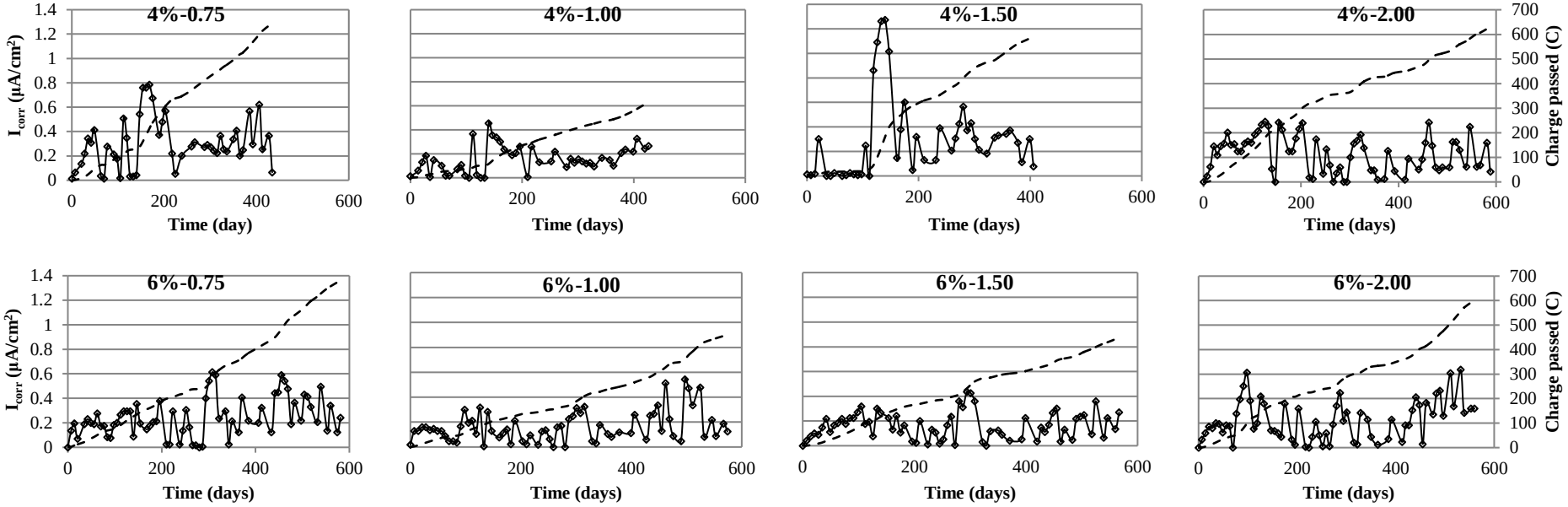
4%-0.75
4%-1.00
4%-1.50
4%-2.00
6%-0.75
6%-1.00
6%-1.50
6%-2.00
I_{corr} (µA/cm²)
Charge passed (C)
Time (day)
Time (days)
0
200
400
600
0.2
0.4
0.6
0.8
1
1.2
1.4
100
300
500
700

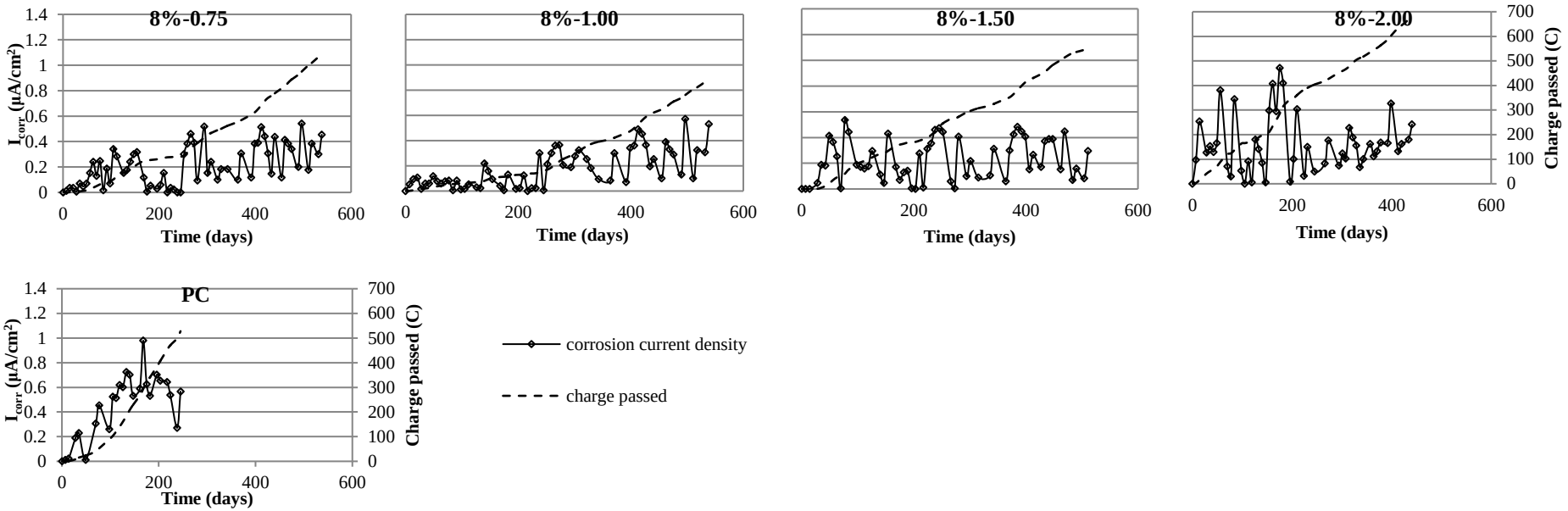

Fig. 4 Corrosion current and charge passed

From Fig. 4 it can be seen that the corrosion current for AAS concrete fluctuates highly, but in general stays lower than that of the PC reference concrete. There is no prolonged initiation period for any of the mixes studied, presumably due to the fairly aggressive cyclic ponding regime and the lower cover depth of 15mm used in this research. The relatively lower alkalinity (Fig. 3) and higher sulphide concentration of the AAS concretes (Ma, *et al*., 2016) could have disrupted the passive film on the surface of the anodic steel, resulting in the early initiation of corrosion (Tennakoon, *et al*., 2017, Pourbaix, 1996, Shoesmith, *et al*., 1978). After the initiation of corrosion, the rate of increase of macrocell current was much lower for the AAS concretes compared to the PC concrete (see Fig. 4). This agrees with the results reported by Holloway and Sykes (2005), in which a very low corrosion current was also found for the AAS concretes. Consequently, the charge passed for the AAS concretes was lower than that of PC reference for similar duration of exposure (see Fig. 4). The following reasons are attributed to the above behaviour:

(a) Previous studies (Ma, *et al*., 2016 and Tennakoon, *et al*., 2017) reported high bulk resistivity and low chloride diffusivity for AAS concretes. As a result, few chlorides should reach the reinforcing steel in AAS concretes to act as a catalyst to increase further depassivation of the steel. The water soluble and the total chloride concentration at the level of the anodic steel for these ponding slabs were measured at the end of the test (see Table 3). It was noted that the total chloride concentration for the AAS concretes was similar to that for the PC concrete irrespective of slightly longer test durations for the former type. Further, the water soluble chloride concentration was notably low for the AAS concretes. Although water soluble chlorides cannot be equated to free chlorides, it could be interpreted that, for a given test duration, lower amounts of chloride were available for further depassivation of the steel in the AAS concretes. This may explain the reason for the low values of macrocell current measured

in AAS concretes. Further, within the AAS concretes, it seems that the bar in the mix of 6%-1.50 had the lowest charge passed at any given time. From previous study (Ma, *et al*., 2016) it is known that this mix had the lowest diffusivity. Further, in Table 3 the chloride content at the level of the steel bar is very low for this concrete. Ma *et al.* (2016) reported that this concrete exhibited high bulk resistivity. All of these together contributed to the low charge passed for this concrete.

(b) Glasser (1991) and Andersson *et al.* (1989) reported the redox potential of slag cement is maintained between -150 and -410mV, due to the presence of sulphides, compared to 100 to 200mV for PC (Hewlett, 2003). Redox potential measurement is a reflection of oxidisation and reduction activities. This decreases to a more negative value with the increase of reduction atmosphere. Therefore, the incorporation of slag should make reducing environment of cement stronger and, therefore, protects the embedded steel from oxidisation and lower the rate of corrosion steel. Besides, the oxidation of chemically reduced sulphides would form elemental sulphur to deposit in the pores of the damaged passive film allowing the corroded steel to regain passivation [23]. Similar to slag cement, large amount of sulphides presents in the AAS concretes [5]. Therefore, the steel in such concretes could also regain passivation as a result of the reduction of sulphides and the repair of passivating film. Recently, Mundra *et al.* (2017) confirmed that the presence of sulphides alter the mechanism of corrosion of steel in simulated AAS pore solution. Initiation and pitting were observed to be governed by the pore solution concentration of sulphides and not the chloride concentration as thought for Portland cement systems.

Table 3 also reports the mass loss of the anodic steel bars in the concretes calculated from the macrocell current and compares the results to the one measured gravimetrically.

Table 3 Total and water soluble chlorides (% by mass of concrete) at the level of the anodic steel after the ponding test and both measured and estimated mass loss of the anodic steel bars

Mix Identify (test duration in days)	**Chlorides (% by mass of concrete)**		**Apparent pH**	**Mass loss (% of the original mass)**		$\frac{\textbf{Calculated}}{\textbf{Measured}}\%$
	Total	**Water soluble**		**Measured**	**Calculated**	
4%-0.75 (434)	0.45	0.31	11.35	0.39	0.07	18
4%-1.00 (427)	0.44	0.21	11.40	0.51	0.04	7.8
4%-1.50 (406)	0.45	0.19	11.72	0.50	0.06	12
4%-2.00 (588)	0.54	0.20	11.66	0.38	0.07	18
6%-0.75 (581)	0.40	0.19	11.88	0.29	0.08	28
6%-1.00 (574)	0.34	0.17	11.76	0.21	0.05	24
6%-1.50 (567)	0.28	0.16	12.16	0.26	0.05	19
6%-2.00 (560)	0.34	0.20	11.81	0.33	0.07	21
8%-0.75 (539)	0.45	0.15	12.17	0.29	0.06	21
8%-1.00 (539)	0.46	0.20	11.91	0.27	0.05	18
8%-1.50 (511)	0.45	0.23	12.17	0.34	0.06	18
8%-2.00 (441)	0.44	0.26	11.92	0.63	0.08	13
PC (245)	0.41	0.20	12.61	0.14	0.06	43

Reliability of I_{corr}

From Table 3 it can be seen that the calculated mass loss based on macrocell current was lower than that obtained from the gravimetric measurement. The mass loss based on corrosion current was between 7.8 and 28% of the gravimetric mass loss for AAS concretes. This ratio was 43% for the PC concrete. In the test set-up in Fig. 1, known commonly as the macrocell corrosion test, the expectation is that all of the top bar will act as the anode and all of the bottom bars will act as the cathode. Therefore, by measuring the current between the anode and the cathode, the macrocell corrosion can be determined. However, this set up does not facilitate the measurement of any microcell corrosion between two locations on the top bar (Andrade, et al., 2004). The uneven or non-uniform penetration of chlorides could result in microcell corrosion between an anodic site and an adjacent cathodic site on the same bar, which could be significant, as was observed for all of the AAS concretes in this research. Unfortunately, the current due to microcell corrosion is not easy to measure, despite being significant for all of the AAS concretes. The non-uniform leaching of alkaline material from AAS concretes, resulting in a low pH at different locations of the embedded steel also might have provided a more conductive environment for developing the microcell corrosion in these concretes, as demonstrated by Monticelli *et al.* (2016) for alkali activated class F fly ash mortar specimens.

Fig. 5 shows corrosion of the steel bars in one of the AAS mixes and the PC reference. Due to the different test duration, the extent of corrosion is not comparable between the AAS and PC concretes. In the macrocell set-up, it was intended to make corrosion distributed onto the surface of the entire anodic steel bar (top bar) approximately uniformly. However, as shown in Fig. 5, this is not particularly true for the bar in the AAS concrete. Obvious pitting (anodic region) is observed locally on the surface of the top bar in the AAS concrete, surrounded by larger uncorroded area acting as the cathode, as shown in Fig. 5(a). The pitting corrosion is

considered to be caused by the microcell mentioned above, confirming that microcell corrosion did play a more important role in the corrosion of the steel bars in the AAS concretes. For the bar in PC concrete, the contribution of the macrocell corrosion to the total mass loss was more compared to the AAS concretes (as shown Table 3), which means that a more uniform distribution of corrosion was expected on the surface of the top bar in PC, in which is confirmed by the finding in Fig. 5(b).

(a) AAS - corrosion evident on the highlighted area surrounded by sound regions, localised pitting evident

(b) PC - corrosion spread over a larger region

Fig. 5 Corrosion of the anodic steel bars (top bars) in one of the AAS mix (4%-1.00) and PC reference

Ionic flow through concrete from cathode to anode is required to set up a corrosion cell. The higher electrical resistivity of the AAS concretes (Ma, *et al*., 2016) and lower diffusivity may have restricted the ionic movement between the electrodes as it does in PC based systems (Dhanya and Santhanam, 2017). This could have favoured the formation of the microcell corrosion in AAS concretes, where anodes and cathodes are formed in the same bar next to each other as compared to macrocell corrosion where anode and cathode are separate bars kept at a distance apart. The distance between the anode and cathode bars must have also played a part in favouring the microcell corrosion. The test set-up in Fig. 1 was adopted from Basheer *et al.* (1998) and is found suitable for PC based systems. In summary, macrocell current measured using this test set-up does not provide a good observation of the corrosion behaviour of AAS concretes. The suitability of macrocell corrosion measurement for PC concrete itself is also questionable given the fact that only 43% of the total corrosion current was due to the macrocell corrosion. This will lead clearly to an underestimation of the corrosion process (Trejo and Monteiro, 2005).

3. 2 Half-cell potential

The evolution of half-cell potential of the anodic steel is presented in Fig. 6. This figure also gives the corrosion risk classification using half-cell potential as specified in American Society for Testing Materials C 876 (2009).

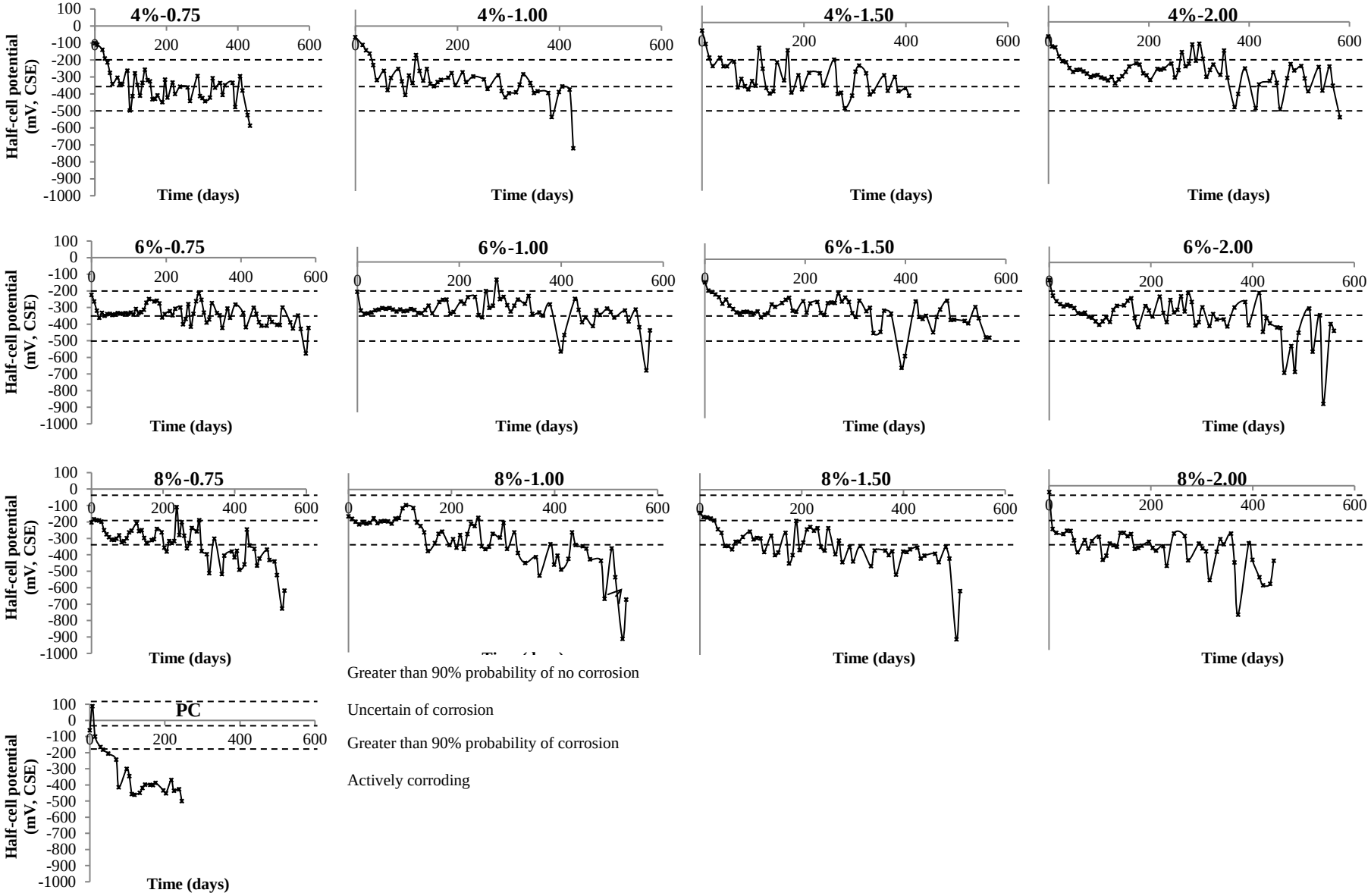
4%-0.75
4%-1.00
4%-1.50
4%-2.00
6%-0.75
6%-1.00
6%-1.50
6%-2.00
8%-0.75
8%-1.00
8%-1.50
8%-2.00
PC
Half-cell potential (mV, CSE)
Time (days)
Greater than 90% probability of no corrosion
Uncertain of corrosion
Greater than 90% probability of corrosion
Actively corroding

Fig. 6 Evolution of half-cell potential of the anodic steel bars

Half-cell potentials can be used to characterise the risk of corrosion in PC based concretes. The more negative the value is, the higher is the corrosion risk. According to the guidelines specified in American Society for Testing Materials C 876 (2009), when half-cell potential is more negative than -200mV, steel bar is at a risk of corrosion. Similar to the results reported in (Tennakoon, *et al*., 2017), a very negative potential value is generally observed for the bars in AAS concretes even at the start of the test. If the ASTM criteria is applied to evaluate these bars, it appears that AAS experience a very severe corrosion. However, the results show that the bars in most of the AAS concretes have a comparable corrosion rate with the bar in PC. As explained by Tennakoon *et al.* (2017), the possible reason for the very negative half-cell potential could be due to the presence of sulphide ions in the pore solution of AAS concretes to reduce the potential values. Consequently, it is questionable to apply the half-cell potential criteria developed for PC concretes for evaluating the corrosion activity of the steel bars in AAS concretes due to such measurement could over-estimate their real corrosion risks.

However, the half-cell potential curves offer similar findings to that of macrocell current results: they are: (a), the anodic steel reacts to the environment early on for AAS concretes; and (b) the rate of reduction of the potential for the AAS concretes was lower compared to the PC reference. This confirms that the corrosion of steel in AAS concretes was initiated at an early stage, while after that, the steel regained passivity to a greater extent. The possible reasons for this have been discussed in the previous section.

4. Conclusions

On the basis of the mixes studied and the tests carried out for the work reported in this paper, the following conclusions have been drawn:

- Corrosion initiates early for AAS concretes despite the low diffusivity and low levels of water soluble chloride concentration. The possible reasons for this observation could be: (a) the lower alkalinity of the AAS concretes and (b) the higher concentration of sulphides in the AAS concretes.
- Further to the early initiation, the rate of corrosion based on mass loss measurements is comparable to the PC reference concrete. Several factors could be considered responsible for this phase of corrosion, including the low levels of water soluble chlorides present in the pore solution, the higher bulk resistivity restricting the flow of ions from cathode to anode, and regaining the passivity of the steel due to the reduction reaction in presence of sulphides.
- In a typical macrocell test set-up, microcell corrosion is more likely to occur in the AAS concretes due to their high bulk resistivity. In this work, macrocell current measurements underestimated the extent of corrosion of the steel in the AAS concretes. Only 7.8%-28% of corrosion mass loss was accounted for by the macrocell current for the AAS concretes.
- Conforming to the redox potential values reported for slag based systems, the half-cell potential for AAS concretes remain negative from the start. The rate of decrease of half-cell potential in AAS concretes is much lower than that in PC reference, but it is questionable to apply the half-cell potential criteria developed for PC concretes for evaluating the corrosion risk of the steel in the AAS concretes.

Note that these findings are intended to demonstrate the differential behaviour of AAS mixes compared to Portland systems. However, a detailed investigation to establish the significance

of mix variables and the role played by sulphides is recommended. The authors suggest a factorial experimental design so that both the main and interactive effects of factors could be established for all of the properties measured.

Acknowledgements

The authors gratefully acknowledge the funding by the EPSRC as part of the UK-China Science Bridge project (EPSRC/G042594/1) and China Scholarship Council. They also acknowledge the support by Queen's University Belfast and University of Leeds for carrying out the experimental work and the EPSRC funding (EP/M003272/1) for the time to prepare and review this article. We also thank Kunming University of Science and Technology for the time allocated to first author for the preparation of this paper. The slag used in this research was supplied by Civil and Marine Ltd.. Dr. Qianmin Ma has been sponsored also by the National Natural Science Foundation of China (NNSFC, Grant Nos.: 52068038, 51502121) and Yunnan Provincial Department of Education (Grant No: 2019J0044). All of these are gratefully acknowledged. The experimental work described in this article was carried out between 2010 and 2013.

Compliance with ethical standards

Conflict of interest

The authors declare that they have no conflict of interest.

Reference

Al-Otaibi, S. (2008), 'Durability of concrete incorporating GGBS activated by water-glass', *Construction and Building Materials*, Vol. 22, pp. 2059-2067.

American Society for Testing of Materials, C 876 (2009), *Standard test method for half-cell potentials of uncoated reinforcing steel in concrete*, ASTM International.

Andersson, K., Allard, B., Bengtsson, M. and Magnusson, B. (1989), 'Chemical composition of cement pore solutions', *Cement and Concrete Research*, Vol. 19(3), pp. 327-332.

Andrade, C., Alonso, C., Gulikers, J., Polder, R., Cigna, R., Vennesland, O., Salta, M., Raharinaivo, A. and Elsener, B. (2004), RILEM TC 154-EMC: 'Electrochemial techniques for measuring metallic corrosion' Recommendations Test methods for on-site corrosion rate measurement of steel reinforcement in concrete by means of the polarization resistance method, *Materials and Structures*, Vol. 37, pp. 623-643.

Basheer, L., Cleland, D.J. and Long, A.E. (1998), 'Protection provided by surface treatments against chloride induced corrosion', Materials and Structures, Vol. 31, pp. 459-464.

British Standard 1881-125 (1986), *Testing concrete-Part 125: Methods for mixing and sampling fresh concrete in the laboratory*, British Standards Institution.

British Standard EN197-1 (2000), *Cement-Part 1: Composition, specifications and conformity criteria for common cements*, British Standards Institution.

British Standard EN206-1 (2000), *Concrete-Part 1: Specification, performance, production and conformity*, British Standards Institution.

British Standard 8500-1 (2006), *Concrete-complementary British Standard to BS EN 206-1: method of specifying and guidance for the specifier*, British Standards Institution.

British Standard EN 12350-2 (2009), *Testing fresh concrete Part 2:Slump-test*, British Standards Institution.

British Standard EN 12350-3 (2009), *Testing hardened concrete Part 3:Compressive strength of test specimens*, British Standards Institution.

Broomfield, J.P. (2007), *Corrosion of steel in concrete: understanding, investigation and repair*, Taylor & Francis, London.

Criado, M. and Provis, J.L. (2018), 'Alkali activated slag mortars provide high resistance to chloride-induced corrosion of steel', Frontiers of Materials, 5.34, doi: 10.3389/fmats.2018.00034.

Dhanya, B.S. and Santhanam, M. (2017), 'Performance evaluation of rapid chloride permeability test in concretes with supplementary cementitious materials', *Materials and Structures*, Vol. 50 (67).

Glasser, F.P. (1991), 'Chemical, mineralogical, and microstructural changes occurring in hydrated slag-cement blends', *Material Science of Concrete* II, pp. 41-81.

Hewlett, P.C. (2003), *Lea's chemistry of cement and concrete*. Elsevier Science & Technology Books, Amsterdam.

Holloway, M. and Sykes, J.M. (2005), 'Studies of the corrosion of mild steel in alkali-activated slag cement mortars with sodium chloride admixtures by a galvanostatic pulse method', *Corrosion Science*, Vol. 47, pp. 3097-3110.

Johannesson, B., Yamada, K., Nilsson, L-O. and Hosokawa, Y. (2007), 'Multi-species ionic diffusion in concrete with account to interaction between ions in the pore solution and the cement hydrates', *Materials and Structures*, Vol. 40, pp. 51-665.

Ma, Q., Nanukuttan, S.V., Basheer, P.A.M., Bai, Y. and Yang, C. (2016), 'Chloride transport and the resulting corrosion of steel bars in alkali activated slag concretes', *Materials and Structures*, Vol. 49, pp. 3663-3677.

Monticelli, C., Natali, M.E., Balbo, A., Chiavari, C., Zanotto, F., Manzi, S. and Bignozzi, M.C. (2016), 'A study of the corrosion of reinforcing bars in alkali-activated fly ash mortars under wet and dry exposures to chloride solutions', *Cement and Concrete Research*, Vol. 87, pp. 53-63.

Mundra, S., Bernal, S. and Provis, J. (2017), 'Corrosion initiation of steel reinforcement in simulated alkali-activated slag pore solutions', 1st International Conference on Construction Materials for Sustainable Future, 19-21 April 2017, Zadar, Croatia.

Pourbaix, M. (1966), *Atlas of electrochemical equilibria in aqueous solutions*, Pergamon Press, Oxford.

Ravikumar, D. and Neithalath, N. (2013), 'Electrically induced chloride ion transport in alkali activated slag concretes and the influence of microstructure', *Cement and Concrete Research*, Vol. 47, pp. 31-42.

RILEM TC 178-TMC (2002a), 'Testing and modelling chloride penetration in concrete' analysis of total chloride content in concrete recommendation', *Materials and Structures*, Vol. 35, pp. 583–585.

RILEM TC 178-TMC (2002b), 'Testing and modelling chloride penetration in concrete' Analysis of water soluble chloride content in concrete recommendation', *Materials and Structures*, Vol. 35, pp. 586-588.

Runci, A. and Serdar, M. (2020), 'Chloride-induced corrosion of steel in alkali-activated mortars based on different precursors', *Materials*, Vol. 13(22), doi:10.3390/ma13225244.

Shi, C., Krivenko, P.V. and Roy, D. (2006), *Alkali-Activated Cements and Concretes*, Taylor & Francis, London.

Shoesmith, D.W., Taylor, P., Bailey, M.G. and Ikeda, B. (1978), 'Electrochemical behaviour of iron in alkaline sulphide solutions', *Electrochimca Acta*, Vol. 23, pp. 903-916.

Tennakoon, C., Shayan, A., Sanjayan, J.G. and Xu, A. (2017), 'Chloride ingress and steel corrosion in geopolymer concrete based on long term tests', *Materials and Design*, Vol. 116, pp. 287-299.

Torres-Carrasco, M., Tognonvi, M.T., Tagnit-Hamou, A. and Puertas, F (2015), 'Durability of alkali-activated slag concretes prepared using waste glass as alternative activator*'. ACI Materials Journal*, Vol. 112, pp. 791-800.

Trejo, D. and Monteiro, P.J. (2005), 'Corrosion performance of conventional (ASTM A615) and low-alloy (ASTM A706) reinforcing bars embedded in concrete and exposed to chloride environments', *Cement and Concrete Research*, Vol. 35, pp. 562-571.

Yang, C. and Pu, X. (1993), 'Retarder of alkali activated slag', *Chinese patent* 91108316.2.

You, N., Shi, J. and Zhang, Y. (2020), 'Corrosion behaviour of low-carbon steel reinforcement in alkali-activated slag-steel slag and Portland cement-based mortars under simulated marine environment', *Corrosion Science*, Vol. 175, Article No. 108874.